I&EC research
Industrial & Engineering Chemistry Research

pubs.acs.org/IECR

Article

CO_2 and HDPE Upcycling: A Plasma Catalysis Alternative

Fnu Gorky, Apolo Nambo, Travis J. Kessler, J. Hunter Mack, and Maria L. Carreon*

Cite This: *Ind. Eng. Chem. Res.* 2023, 62, 19571−19584

Read Online

ACCESS | Metrics & More | Article Recommendations | Supporting Information

Downloaded via UNIV OF ARKANSAS on July 3, 2024 at 00:50:16 (UTC).
See https://pubs.acs.org/sharingguidelines for options on how to legitimately share published articles.

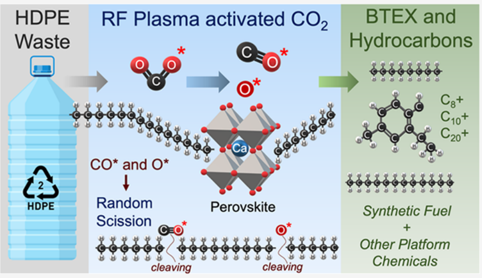

ABSTRACT: This work describes the use of CO_2 plasma as an active directing agent toward high-density polyethylene (HDPE) decomposition to synthetic fuels. We present for the first time the possibility of taking advantage of the electric field when using perovskites, a material responsive to such types of electrical inducement. Perovskites are observed to provide control of the reactive species by increasing the adsorption of the plasma-polarized CO_2 due to their polar crystallographic unit cell that can generate an electric polarization modulated by the external electric field. Moreover, the plasma exposure charges the perovskite surface, and the accumulation of electrons promotes the generation of oxygen vacancies and thus a high conversion of CO_2. The perovskite then leads to an improved intensity of the plasma-generated species prone to initiating HDPE decomposition such as O atoms and CO. This plasma-generated initiator directs random scissions, resulting in condensates that have the potential to be used as synthetic fuels as our product stream contains C_5-C_{11} hydrocarbons similar to naphtha, which can be blended into gasoline; C_9-C_{20} hydrocarbons with higher cetane numbers, similar to diesel; and C_{20+} waxes, which can also be converted into alternative fuel diesel through hydrocracking. We expect this work to initiate the development of tailored materials responsive to electric fields for important sustainable applications, where CO_2 might play an important role.

1. INTRODUCTION

Carbon dioxide is a major air pollutant released into the Earth's atmosphere by the combustion of fossil fuels and is an unavoidable byproduct of a carbon-based economy.[1,2] It contributes to global warming, ocean acidification, and loss of coastal habitat.[3] Future strategies to combat global warming must focus on energy security while reducing greenhouse-gas emissions.[4] Because greenhouse gases have a cumulative effect, a simple reduction in CO_2 emissions will not suffice. Rather, an active removal of CO_2 and new utilization pathways are potentially required.[5]

Another important source of environmental contamination in recent years includes plastics. The use of plastics has increased dramatically and is expected to surge. Plastics are common synthetic polymers extensively employed in industrial sectors and commercial goods.[6] Plastics are composed of a carbon backbone with repeating subunits. Different types of plastics are divided based on their application, such as the family of polyolefins, consisting of polyethylene (high-density polyethylene, HDPE), low-density polyethylene (LDPE), and polypropylene (PP). Based on a 2017 report, out of 6300 Mt of generated plastic waste, 79% was disposed of in landfills, around 9% was recycled, and the remaining 12% was incinerated. Moreover, considering the current production trend, approximately 12,000 Mt of plastic waste will end up in landfills by 2050.[7] The accumulation of plastics has resulted in detrimental environmental effects,[8] with important negative impacts on marine life.[9] It is then essential to find a sustainable route to an efficient plastic deconstruction process. Plastic products made from HDPE are highly convenient due to their versatility, lightweight, and low price. As a result, their use has increased by 20-fold in the past 60 years and has resulted in a corresponding increase of waste.[10] In terms of environmental impact, the EPA (U.S. Environmental Protection Agency) estimates that the global carbon footprint of plastic waste is somewhere between 100 and 300 million tonnes of CO_2 equivalent. To put those figures into context, the plastic waste carbon footprint is equivalent to the carbon emissions of 21−63 million cars driven for one year.[11] Specifically, municipal plastic waste (MPW) comprises a mixture of thermoplastics (high- and low-density polyethylene, HDPE and LDPE; polypropylene, PP; polystyrene, PS; and poly(ethylene terephthalate), PET). Currently, there is a critical need to explore alternative routes for repurposing commodity plastics such as HDPE due to its ubiquity, as it is used in water bottles, piping, milk jugs, and many other common goods. Intensive efforts have been made to recycle HDPE plastic waste. In fact, the current dominant technology for HDPE reprocessing is mechanical recycling, which has been commercialized successfully.[12] However, the global recycling rate is not as high as needed to be environmentally and

Received: July 18, 2023
Revised: October 21, 2023
Accepted: October 24, 2023
Published: November 3, 2023

© 2023 American Chemical Society

https://doi.org/10.1021/acs.iecr.3c02403
Ind. Eng. Chem. Res. 2023, 62, 19571−19584

economically impactful.[13] For example, the end-of-life recycling rate of PE plastic wastes in the United States is only around 9%.[14] The main reason for this low percentage is the limited use of HDPE recycled plastic since it cannot be used in its original applications.[15−17] Therefore, novel approaches that can generate high-value products are desired to spur interest in the reuse of HDPE waste.

Advanced upcycling involves the transformation of waste plastic into value-added products such as hydrogen, light hydrocarbons, and monomers, which can be used either as direct fuels for power generation or as intermediates for the synthesis of chemicals. In fact, raw materials are responsible for 60−90% of the production costs of a chemical industry process. Inexpensive feedstocks produced from chemical recycling could enable a new pathway to lower the manufacturing costs.[18,19]

Specifically, the popularity of HDPE is due to its malleability (low melting point of around 130 °C), resistance to corrosion, and a high strength-to-density ratio. Furthermore, looking at the chemical structure of HDPE, $(C_2H_4)_n$, its potential for creating a variety of fuel products is clear since it is composed of hydrogen and carbon.

Chemical upcycling has played a promising role in the degradation of plastic waste in recent years.[20−25] In this respect, conventional thermal catalytic pyrolysis is a mature technology with extensive literature, well-reported optimum operating parameters,[26−30] kinetic simulations,[31−35] and optimum operating conditions and product composition, specifically to produce waxes, long-chain hydrocarbons, and solid residues.[36−39] Such intensive studies demonstrate that pyrolysis can successfully convert HDPE waste into wax/liquid/oil, although these products require further upgrading to replace fossil fuels. The distribution of hydrocarbons in the wax fraction from thermal pyrolysis makes it a low-quality product due to the high viscosity and high boiling point temperature range, which is not suitable to be used as a fuel without further processing. Further, the high viscosity of the wax fraction prevents its flow downstream and may cause blockages along pipelines unless heated, therefore increasing operation costs.

Recently, the use of catalytic cold plasma-assisted decomposition of HDPE has been reported as a promising alternative for the enhanced production of ethylene at mild (pressure, temperature, and power) conditions.[40] Moreover, nonthermal plasma is well-recognized as one of the feasible technologies that can tailor the pyrolysis product selectivity.[24,41] Nonthermal plasma reactors are lightweight, offer high automation, excellent safety operation, and great potential for scale-up.[42,43] More importantly, nonthermal plasma systems are operated with an electricity source and, thereby, can be efficiently integrated with renewable sources such as wind and solar. These integrated processes can be foreseen as a means for chemical energy storage by using excess electricity from renewable energy sources to produce chemicals from plastic waste. In a plasma reactor, a vast number of excited and dissociated species are generated, and by interaction with an active surface, targeted products can be obtained.[44,45] When comparing the plasma pathway versus the pyrolysis and the thermal catalytic pathway in terms of HDPE activation (chain length reduction), the differences become evident. In the conventional pyrolysis pathway, there is a random chain scission during the carbocation mechanism,[32,46,47] while in catalytic pyrolysis, the β-scission step is dominant and promotes the formation of smaller chains,[47−49] which enhances the formation of lighter compounds, i.e., increases the gas yield. However, for the case of plasma catalysis, it has been recently reported that reduced chain length hydrocarbons, when employing a silica porous-based catalyst, result in the efficient synthesis of light compounds such as alcohols and aldehydes.[50] Hence, herein, we present the use of CO_2 plasma to aid with the production of synthetic fuels from HDPE by random scission favored by the presence of a plasma enhancer.

Previous works have explored the plasma catalytic decomposition of HDPE with nonthermal atmospheric DBD plasma when employing an acid catalyst HZSM-5 zeolite, which favored the formation of light or gaseous hydrocarbons.[51] This motivated us to pursue the understanding of the product formation in a more homogeneous plasma environment (radio frequency plasma) using a greenhouse gas (GHG) CO_2, a mild oxidant, by exploring various alkaline earth metal perovskites ($MgTiO_3$, $CaTiO_3$, $SrTiO_3$, $BaTiO_3$) as plasma enhancers. The main driving force behind using the presented materials is the absence of acid sites, which has been shown to produce high yields of liquid hydrocarbons.[52] Also, perovskites have a polar crystallographic unit cell (due to a distorted dimensional structure in the bulk)[53] and thus can generate spontaneous, electric polarization, whose direction can be modulated by an external electric field.[54−56] Other plasma-response-boosting properties include a high absorption coefficient, long-range ambipolar charge transport, low exciton-binding energy, high dielectric constant, and ferroelectricity. These properties could improve the perovskite interaction with the RF plasma-generated polarized CO_2 species, which could improve the efficiency of the CO_2 dissociation reaction as the plasma-generated species might be employed efficiently by a plasma-activated material.[57,58] Chemical properties that make a perovskite attractive for plasma-driven CO_2 conversion include their readiness to dissolve hydrogen, which can ease reducibility, resulting in improved catalyst lifetime;[59] high chemical stability; high oxygen mobility, which is important in reducing carbon deposition;[60] and a porous crystalline structure accessible for guest molecule diffusion. Moreover, as plasma exposure charges a solid dielectric surface, in perovskites, the accumulation of electrons on the surface could lead to oxide reduction, generation of oxygen vacancies, and thus a high reduction of CO_2.[61] Hence, our major focus in this work is to experimentally investigate the evolution of condensates formed during plasma CO_2-mediated HDPE decomposition and further apply predictive models (artificial neural networks) to verify combustion properties. The investigations into synthetic fuel (liquid fraction) using alternative electrified methods are presently critical as a major strategy to mitigate anthropogenic CO_2 emissions.[62] Interestingly, one of the common applications of the presented work is the synthesis of sustainable aviation fuel,[63] where the presence of aromatic compounds (aromatic range 8−25%)[64] is critical. The importance of chemical upcycling has already been highlighted. This work presents the utilization of CO_2, a major GHG, toward HDPE decomposition with low-temperature plasma processing for promoting carbon circularity[65] by reducing the carbon footprint and thus having a positive impact on climate change.[66] It presents the use of a material that can uniquely take advantage of the plasma environment, helping us set the initial steps to address the question about the use of the same traditional materials employed in thermal catalysis to be applied in plasma catalytic processes.

2. EXPERIMENTAL SECTION

2.1. Materials. Pure HDPE pellets were purchased from Sigma-Aldrich, with melt index 12 g/10 min (190 °C/2.16 kg) and CAS number 427985. The employed catalysts were purchased from Alfa Aesar and ACROS Organics: $MgTiO_3$ (Alfa Aesar, 11 398, magnesium titanium oxide, 99% (metal basis)), $CaTiO_3$ (Alfa Aesar, 11 397, calcium titanium oxide, 99+% (metal basis)), $SrTiO_3$ (Alfa Aesar, 11 399, strontium titanium oxide, 99+% (metal basis)), and $BaTiO_3$ (barium titanate(IV), 99%, ACROS Organics).

The tailored $CaTiO_3$ samples were synthesized by a hydrothermal method adapted from elsewhere.[67] Briefly, calcium nitrate ($Ca(NO_3)_2 \cdot 4H_2O$) (2.362 g) was dissolved in 50 mL of water in a beaker and continuously stirred at 25 °C. 3.4 mL of tetrabutyl titanate ($Ti(C_4H_9O)_4$) was added dropwise into the solution under vigorous stirring, proceeded by the minor addition of NaOH (0.6 g) for mineralization and homogeneous crystal size.[68] The mixture was stirred at 25 °C for 1 h before being transferred to a Teflon-lined stainless steel vessel with 30% headspace. Afterward, it was treated at 200 °C for 24 h. After natural cooling, the precipitates were recovered by centrifugation for 10 min at 5000 rpm, washed three times with deionized water, and further dried under a vacuum at 90 °C for 12 h.

2.2. Perovskite Characterization. The employed catalysts were degassed at 150 °C under a vacuum for 3 h for commercial catalysts and 9 h of lab-synthesized catalysts. Nitrogen physisorption isotherms were conducted at 77 K (ASAP 2020 Plus, Micrometrics) to determine the Brunauer−Emmett−Teller (BET) surface area and particle size (μm) for fresh and plasma-exposed catalysts with nitrogen isotherms (please see Table S1 and Figures S1−S2). The average crystal size for $MgTiO_3$ and $SrTiO_3$ showed a slight increase for the spent catalysts as compared with the fresh catalysts. However, a smaller decrease was observed in the cases of $CaTiO_3$ and $BaTiO_3$. The commercial and tailored perovskites were characterized by powder X-ray diffraction (XRD), with a Bruker Discovery D8 HR-XRD, with the Cu Kα radiation (λ = 1.54 Å) ranging from 10 to 90° angles for confirming the XRD pattern on the employed catalyst. The scale for intensity (au) was homogenized for all of the employed catalysts for determining their accurate crystallinity (see Supporting Information Figure S3). The morphology of the catalysts was characterized via scanning electron microscopy (SEM) by using a TESCAN Vega3 SEM. The SEM images were collected at an accelerating voltage of 10 kV (please see fresh catalyst in Figure 1 and spent catalyst in Figure S4).

2.3. CO_2 Plasma HDPE Decomposition Setup. The experiments were performed in an in-house-built RF plasma reactor (see Figure 2(a)). The reaction was carried out using CO_2 (Airgas, 99.99%) at different flow rates ranging from 5 to 100 sccm; the reaction chamber was fed using a mass flow controller (MFC). The plasma was generated using an RF power supply with a Matching Network from Seren IPS, Inc. The typical reaction plasma power, pressure, and temperature were 150 W, 0.3 Torr, and 250 °C, respectively, consistent for all experiments. The mentioned parameters were selected based on a preliminary experimental study to achieve the lower input to carry out the decomposition reaction for the presented setup. The vacuum was maintained using an Edwards Dry scroll pump (nXDS6i). The plasma excitation was initiated when the furnace reached the desired temperature. The mass of the HDPE and perovskite loaded was 1 g each, consistent for all reactions. In this study, two different stage setups were constructed for plasma catalytic HDPE decomposition. In the first one, different perovskites with HDPE were loaded into soda-lime glass pipettes plugged with glass wool (see Figure 2(b)); in an alternative setup, different perovskites and HDPE were packed in a porcelain combustion boat (see Figure 2(c)). The vacuum pump's exit was connected to a series of condensers (ice traps) for the collection of liquid condensates, which were further quantified using an Agilent MSD 5975 MS using MassHunter software. The CO_2 conversions were quantified during the reaction using an online Agilent 8860 A GC connected with an HP-PLOTU column (30 m × 0.32 mm × 10 μm) and hydrogen as the carrier gas. All experiments were repeated in triplicates. All-important plasma species were analyzed using optical emission spectroscopy (OES), the light emitted from the discharge was led through an optical system, and the emission spectra of the glow region were measured at the center of the tube, where the reaction was taking place (perovskite + HDPE). The measurements were recorded by using a dual-channel ultraviolet−visible−nearinfrared (UV−vis-NIR) spectrophotometer in the scope mode (Avantes Inc., USB2000 Series). The spectral range was from 200 to 1100 nm, using a line grating of 600 lines/mm and a resolution of 0.4 nm. A bifurcated fiber optic cable of 400 μm was employed. Based on the optimum spectroscopy collection, the integration time was set at 5 s with 100 averaging on AvaSoft software, consistent with our previous works.[69]

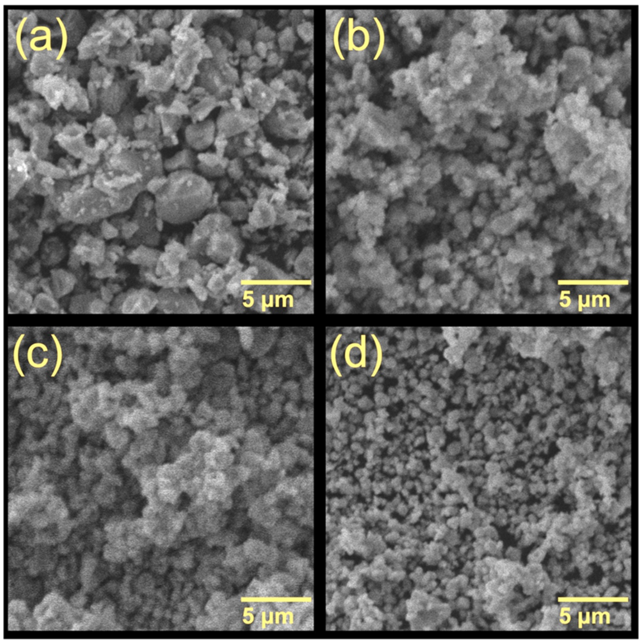

Figure 1. SEM images of fresh (pristine) commercial perovskites employed in this study: (a) $MgTiO_3$, (b) $CaTiO_3$, (c) $SrTiO_3$, and (d) $BaTiO_3$.

2.4. Fuel Property Predictions. Computational approaches have been used extensively to predict molecular properties, including those related to fuels and combustion. Ignition properties, such as cetane number (CN), were initially predicted through linear or nonlinear models for different molecular classes.[70] However, the accuracy and applicability of these models have been quickly surpassed by approaches based on machine learning, especially those that employ artificial

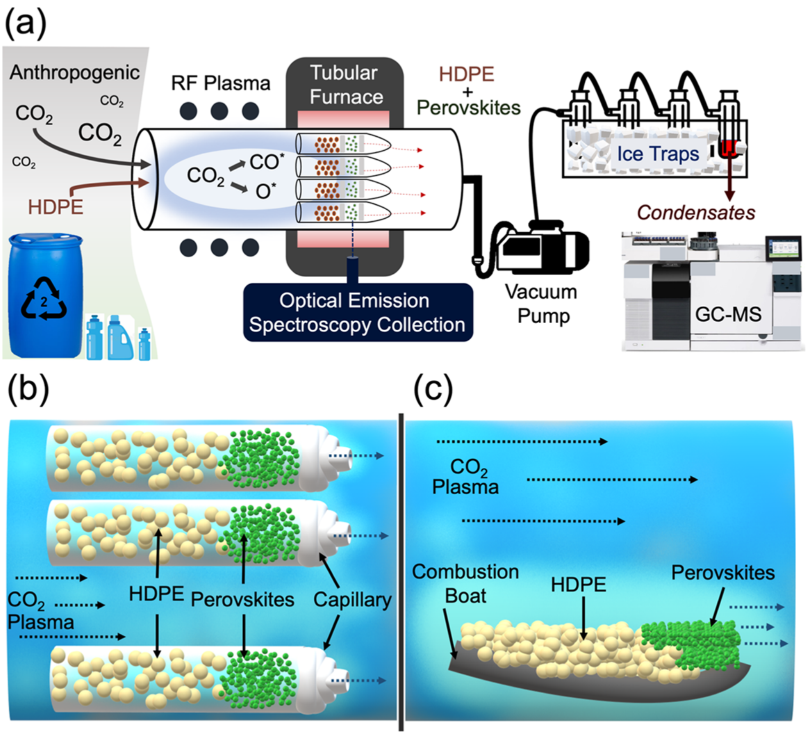

Figure 2. (a) RF plasma HDPE decomposition schematics, (b) stage setup with HDPE and catalyst packed inside a glass capillary, and (c) stage setup with HDPE and catalyst packed on a combustion boat.

neural networks (ANNs).[71] Inputs for such models can include physical properties, spectroscopy, and functional groups.[72−74] An effective approach includes the use of quantitative structure−property relationship (QSPR) descriptors as inputs for molecules of interest. QSPR descriptors are quantifiable characteristics used to describe various chemical and physical properties of a given compound, such as molecular weight, the number of carbon atoms, and the frequency of rings for a given compound. The approach has been used to predict the CN,[75] the yield sooting index (YSI),[76] the flash point,[70] kinematic viscosity (KV),[77] and cloud point (CP)[78] of individual species.

Models that leverage machine learning techniques have used different approaches, including artificial neural networks (ANNs), graph neural networks (GNNs), and convolutional neural networks.[79−81] GNNs are generally more interpretable with respect to input-target relationships, while ANNs typically have a higher degree of accuracy. The ANN-based approach presented here has been detailed in several previous publications, including data preprocessing, QSPR descriptor generation, QSPR descriptor downselection, and ANN training.[82,83]

Predictive models can be used in series with known equations to model the behavior of multicomponent blends during combustion. While properties like CN, LHV, and YSI are proportionally linear with respect to the volume fractions of the individual components, KV and CP are shown to be inversely logarithmic and inversely exponential, respectively, with respect to volume fraction. The specific equations used, as well as an outline of the overall predictive pipeline, are available in a previously published work.[84]

3. RESULTS AND DISCUSSION

3.1. Plasma Catalytic Performance.

Figure 3 shows the CO_2 conversion as a function of time. The CO_2 conversions were calculated using eq 1; prior to experimental data collection, the CO_2 calibration curve was developed to quantify the unknown flow rates (sccm).

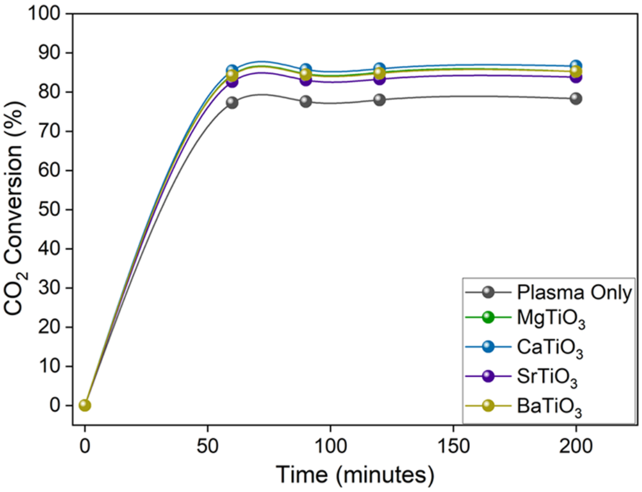

Figure 3. CO_2 conversion as a function of time for plasma-only and different perovskites at a total flow rate of 10 sccm, pressure of 0.3 Torr, plasma power of 150 W, and temperature of 250 °C.

$$\text{CO}_2\text{ conversion }(\%)\frac{\text{CO}_2(\text{inlet})-\text{CO}_2(\text{outlet})}{\text{CO}_2(\text{inlet})}\times 100 \quad (\%) \tag{1}$$

It is evident that CO_2 plasma activation is very effective to promote the degradation reaction of HDPE. In all cases, we could observe a CO_2 conversion above 70%. While the plasma-only system achieves the lowest conversion, it is not far behind that of the perovskite systems. To analyze the impact of the

Table 1. Liquid Condensate Product Analysis via GC-MS

S. No.	Products GC-MS	RT Retention Time minutes	MW Molecular Weight g/mol	Chemical Formula	Chain	Structure	^Applications	#Ref.
1	2-methyl-Octane	6.506	128.25	C_9H_{20}	C9	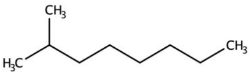	Fuel Component	85-87
2	2-ethyl-1,4-dimethyl-Benzene	8.779	134.21	$C_{10}H_{14}$	C10+	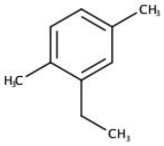	Fuel Component	88-90
3	Naphthalene	9.533	128.17	$C_{10}H_8$	C10	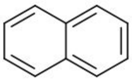	Deodorant block, softener, Fuel Component, plastic and resin production, tanning agents for leather and rubber	91, 92
4	Dodecane	9.808	170.3	$C_{12}H_{26}$	C10+	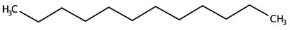	Solvent, hydrogen producer	93-95
5	2,3,6-trimethyl-Decane	11.555	184.36	$C_{13}H_{28}$	C10+	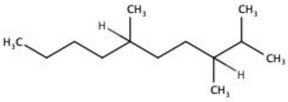	Phase change material	96, 97
6	Tetradecane	13.935	198.39	$C_{14}H_{30}$	C10+	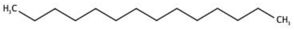	Phase change material, Flavor additive	93, 98, 99
7	2,4-Di-tert-butylphenol	16.017	206.32	$C_{14}H_{22}O$	C10+		Fuel Component	89, 90, 100
8	Tetracosane	19.965	338.7	$C_{24}H_{50}$	C20+	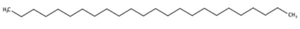	Phase change material	101, 102
9	9-methyl-Nonadecane	21.316	282.5	$C_{20}H_{42}$	C20+	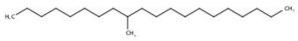	Jet Fuel	100, 103
10	Nonadecane	22.016	268.5	$C_{19}H_{40}$	C10+	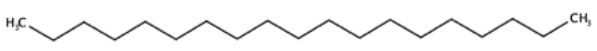	Fragrance component, Phase change material	93, 104, 105

^Applications represent the utilization of the presented liquid condensate reported in the literature. #ref. represents the citations for applications and liquid condensate reported in the literature.

plasma-activated materials, it is important to look further into the product distribution of the condensates.[85−90]

Table 1 shows the main products obtained from the analysis of condensates during plasma decomposition of HDPE when commercial alkaline earth perovskites. For a systematic analysis, the products obtained from the plasma decomposition of HDPE were grouped as medium fraction (containing C5−C9) and diesel/fuel fraction (containing C10+ hydrocarbons).[92−99]

3.2. Time-Resolved Product Analysis. We performed the HDPE decomposition under a CO_2 plasma environment using different alkaline earth commercial perovskites including $MgTiO_3$, $CaTiO_3$, $SrTiO_3$, and $BaTiO_3$ at different reaction times, i.e., 30, 60, 90, and 240 min (see Figure 4). For comparison, we performed the plasma-only reaction or the reaction in the absence of perovskites. From the gas chromatography−mass spectrometry (GC−MS) analysis of the liquid sample as a general trend, we observed that the generation of most of the products was seen to increase in the presence of the perovskites compared with plasma only. Interestingly, when using a perovskite, the formation of all products except for nonadecane ($C_{19}H_{40}$) showed higher values at a longer time (240 min).[100−105] Furthermore, it is possible to observe that our presented route generates straight-

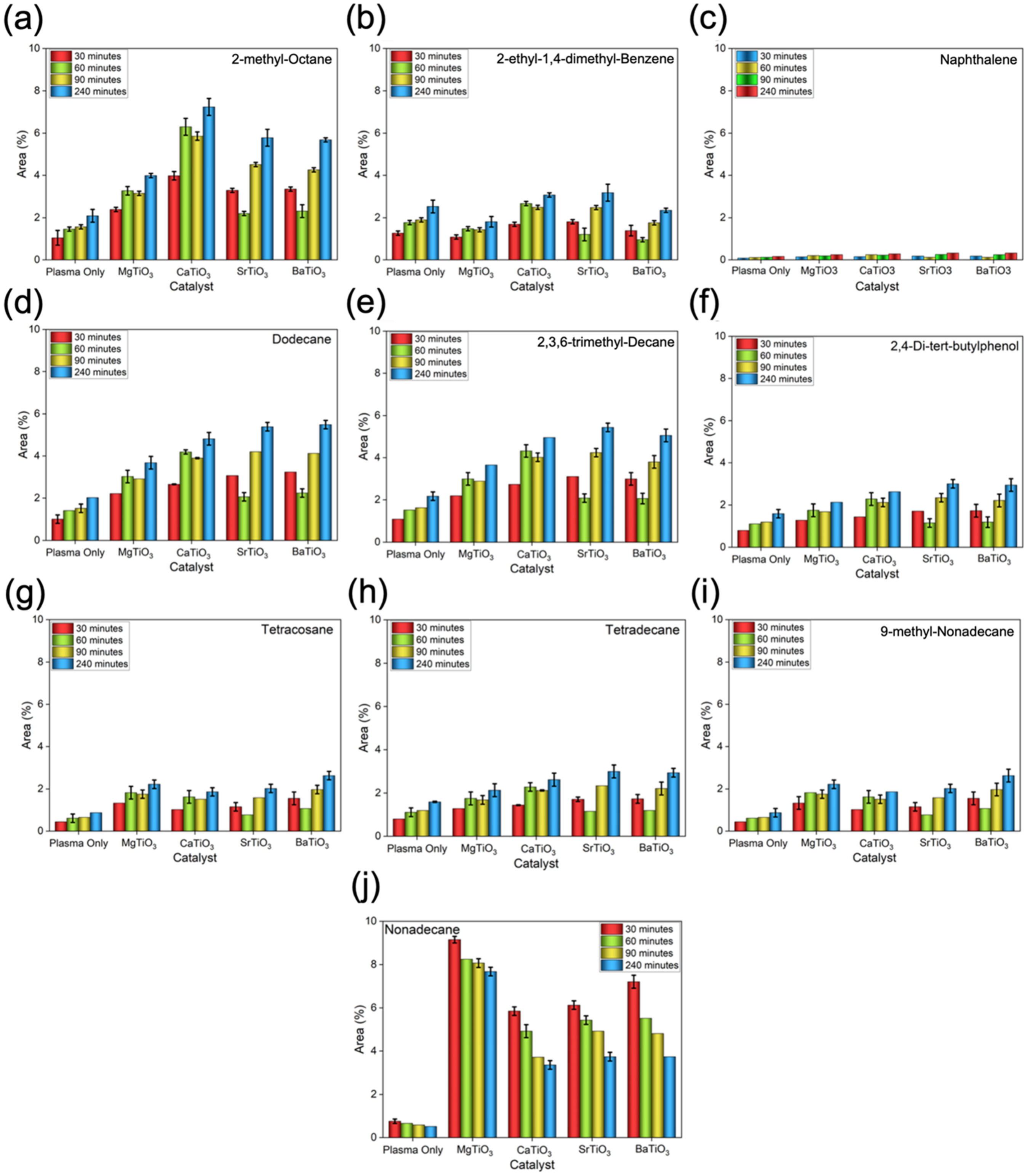

Figure 4. Time-resolved kinetic analysis on HDPE decomposition with various commercial perovskites: $MgTiO_3$, $CaTiO_3$, $SrTiO_3$, and $BaTiO_3$. Compounds listed are (a) 2-methyl-octane, (b) 2-ethyl-1,4-dimethyl-benzene, (c) naphthalene, (d) dodecane, (e) 2,3,6-trimethyl-decane, (f) tetradecane, (g) 2,4-di-*tert*-butylphenol, (h) tetracosane, (i) 9-methyl-nonadecane, and (j) nonadecane.

chain hydrocarbons, which can be further processed into diesel via hydrocracking reactions.[106] The higher yield observed for straight chains could be due to the interaction of the intermediaries with the electric field and the polarized perovskite, thus enhancing the stabilization of the charged species.[107] Specifically, synthetic fuel can be produced from the current product streams generated, comprising C_5-C_{11} naphtha, which can be blended into gasoline; C_9-C_{20} diesel, which has a high cetane number; and C_{20+} waxes, which can also be converted into diesel through hydrocracking. Interestingly, the mixture obtained shows the presence of

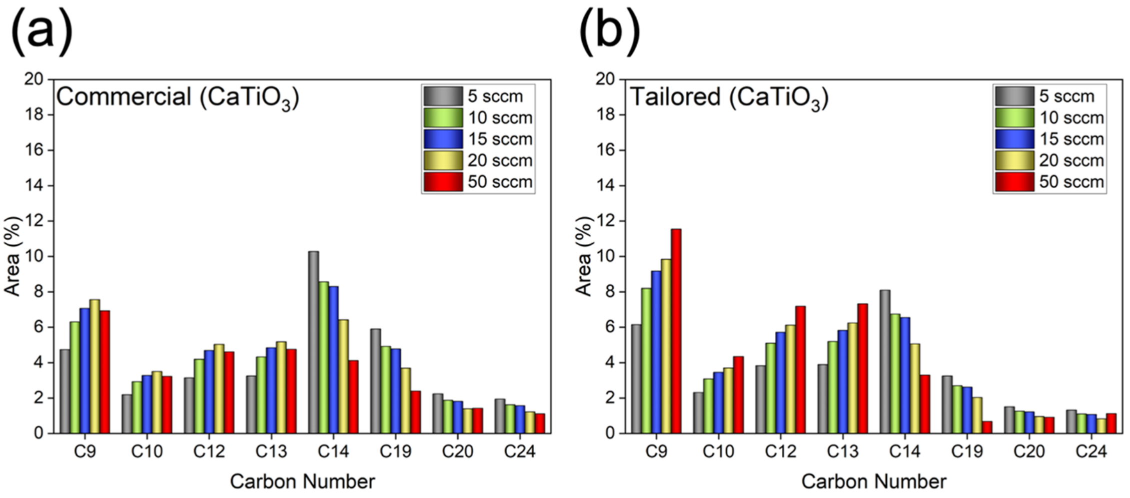

Figure 5. Effect of the perovskite on product distribution for HDPE decomposition when employing (a) commercial vs (b) tailored perovskite ($CaTiO_3$) at various flow rates for 60 min of reaction time.

Table 2. Experimental and Predicted Combustion Properties for Species Present in Liquid Condensates[a]

s. no.	compound	CN (−)	LHV (MJ/kg)	YSI (−)	KV (cSt)
1	2-methyl-octane	39.00	44.29[b]	57.09[b]	0.66
2	2-ethyl-1,4-dimethyl-benzene	3.51[b]	42.28[b]	376.90[b]	0.98[b]
3	naphthalene	22.00	43.83[b]	466.10	1.75[b]
4	dodecane	72.90	44.43[b]	71.70	1.55
5	2,3,6-trimethyl-decane	41.42[b]	44.47[b]	110.29[b]	1.47[b]
6	tetradecane	85.10	44.50[b]	85.31[b]	2.25
7	2,4-di-*tert*-butylphenol	8.71[b]	36.02[b]	468.53[b]	5.29[b]
8	tetracosane	89.84[b]	44.65[b]	193.72[b]	8.29[b]
9	9-methyl-nonadecane	67.50[b]	44.61[b]	154.53[b]	4.70[b]
10	nonadecane	110.0[b]	44.59[b]	125.32[b]	4.70
	diesel fuel[84]	40−55	42.6	235−250	1.9−6.0

[a] Key - CN, cetane number; LHV, lower heating value; YSI, yield sooting index; KV: kinematic viscosity. [b] Denotes a predicted property; see Section 2.4.

benzene, which could possibly influence the octane number and performance characteristics of a fuel.[108]

Moreover, when looking at the plasma-only results (Figure S5, Supporting Information), it is possible to observe that the decomposition of HDPE is doable; however, it benefits by the presence of the perovskite. Specifically, a maximum enhancement in the production of C9 compounds of approximately 5.6 times more is observed for the tailored $CaTiO_3$ perovskite compared with only plasma.

3.3. Effect of Residence Time. Considering the remarkable behavior of $CaTiO_3$ toward the production of important chemicals such as 2-methyl-octane, along with the availability and lower cost of Ca-based catalysts, we performed a detailed analysis at different flow rates, i.e., 5, 10, 15, 20, 50, and 100 scm, at a fixed time of 60 min. For this purpose, we employed commercial $CaTiO_3$ and $CaTiO_3$ tailored or synthesized in our lab. It should be noted that the commercial sample has a BET surface area of 4.95 m^2/g, while the tailored sample shows a BET surface area of 17.51 m^2/g, which is approximately 3.6 times higher than the commercial perovskite. Interestingly, at high flow rates, i.e., 50 sccm, the tailored $CaTiO_3$ perovskite outperforms the commercial one specifically for less than 12 carbon structures such as 2-methyl-octane, 2-ethyl-1,4-dimethyl-benzene, dodecane, and 2,3,6-trimethyl-decane. Values for these products increased at higher flow rates, i.e., from 5 to 50 sccm. The increment for these products (less than 12 carbons in the structure) from 5 sccm to 50 sccm was approximately 1.8 times for the tailored perovskite. The commercial $CaTiO_3$ perovskite with a lower surface area performed the best at the low flow rate of 5 sccm and for the production of long carbon chain products (C14+). Specifically, the generation of products such as 2,4-di-*tert*-butylphenol, tetradecane, tetracosane, 9-methyl-nonadecane, and nonadecane was approximately 2 times higher at 5 sccm than at 50 sccm. It should be noted that the tailored $CaTiO_3$ has a larger surface area and leads to shorter chain products at higher flow rates. It is evident from Figure 5(a,b) that the product distribution is affected by both the residence time and the surface area of the perovskite. The disparity in product distribution with the aid of a catalyst has been widely reported in the literature for thermal and plasma catalysis; please see Table S2.

3.4. Analysis of Liquid Condensates. As shown in Table 1, most of the produced species have been observed in fuels ranging from diesel to jet fuel. Properties relevant to combustion systems for each of these species are given in Table 2. Note that in the absence of literature-reported experimental data, predictive models (see Section 2.4) are employed to fill in data gaps. In order to better understand how processing parameters (catalyst type and reaction time) affect bulk properties, several key combustion properties are then predicted for the blends outlined previously. As shown in

Table 3. Properties Obtained with Commercial vs Tailored Catalysts (Constant Reaction Time of 60 min)[a]

	commercial $CaTiO_3$				tailored $CaTiO_3$			
flow rate (sccm)	predicted CN	predicted LHV (MJ/kg)	predicted YSI	predicted KV (cSt)	predicted CN	predicted LHV (MJ/kg)	predicted YSI	predicted KV (cSt)
5	53.50	42.45	205.65	2.37	50.05	42.64	190.70	1.91
10	52.01	42.77	190.67	2.00	49.20	42.98	173.19	1.64
15	51.53	42.86	185.99	1.90	48.98	43.10	168.34	1.56
20	50.52	43.07	175.80	1.70	48.37	43.24	157.98	1.44
50	49.99	43.29	167.64	1.59	47.53	43.57	145.23	1.28

[a] Key - CN, cetane number; LHV, lower heating value; YSI, yield sooting index; KV, kinematic viscosity.

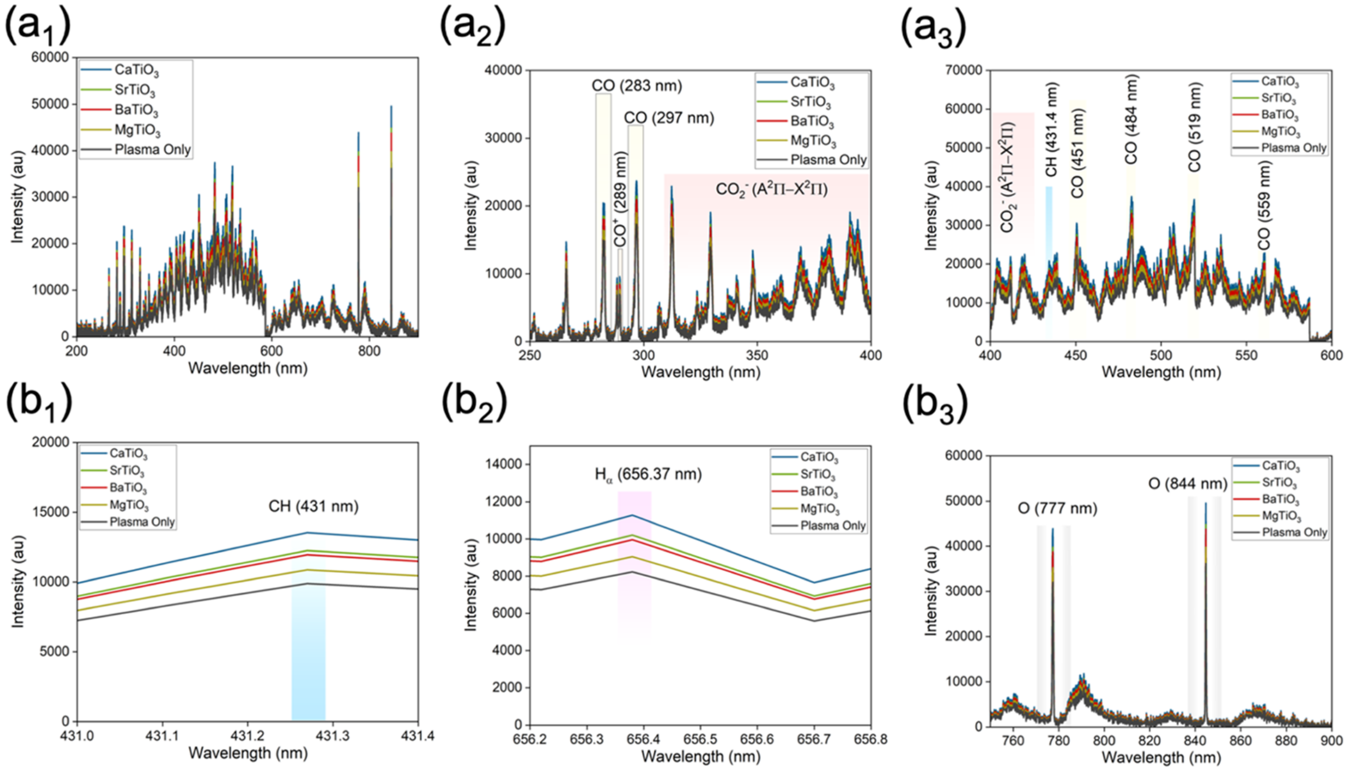

Figure 6. Emission spectra collected during plasma HDPE decomposition for all perovskites ($MgTiO_3$, $CaTiO_3$, $SrTiO_3$, $BaTiO_3$) and plasma only at a 10 sccm flow rate of CO_2; (a) main spectra from 200 to 900 nm; (b) major peaks of important plasma species (CO, CO_2) from 250 to 400 nm; (c) major peaks of important plasma species (CO, CO_2, CH) from 400 to 600 nm; (d) individual peak for the CH band (431.4 nm); (e) individual peak for the H_α band (656.3 nm); and (f) individual peak for molecular oxygen bands (777 and 844 nm).

Table S3, the inclusion of the catalyst consistently produces blends with higher CN, high LHV, and lower YSI. Furthermore, a comparison between commercial and tailored catalysts is shown in Table 3. Predictive model errors, determined by measuring the median absolute errors for unseen test subsets, are expected to be within 5% of the experimental values for all properties given the experimental property ranges.

Based on the single-component data shown in Table 2, it is evident that processes that favor the production of 2-ethyl-1,4-dimethyl-benzene or 2,4-di-*tert*-butylphenol will ultimately be less desirable as a diesel fuel due to their extremely low CN and high YSI values. Conversely, processes that are biased toward creating dodecane and nonadecane, compounds already found in diesel fuel, have an advantage due to their high CN and low YSI. Overall, however, the blends possess favorable overall properties, clearing the baseline values for CN, LHV, and YSI shown in Table 2. High CN mixtures are favorable in blending scenarios since they can be used to raise the CN of lower-quality fuels into the desired range while improving the sooting propensity (lower YSI) without an energy density penalty.

3.5. Mechanistic Insight.

To understand better the plasma gas phase, we performed emission spectra collection (see Figure 6 and Table 4). Interestingly, the intensity of the detected plasma species was observed to be higher when a perovskite is placed inside the reaction chamber than in its absence; this enhancement in the plasma-generated species is due to the strong electric field-perovskite-CO_2 plasma. Such an improvement in the reactive species leads to a higher production of condensates when a perovskite is in the reactor.

The decomposition of HDPE aided by the perovskite-plasma effect can be explained by the carbocation rearrangements, which are common in organic chemistry. They are defined as the movement of any cation containing an even number of electrons, in which a significant portion of the positive charge resides on a carbon atom, from an unstable state to a more stable state through various structural

Table 4. Important Species Detected during CO_2 Plasma HDPE Decomposition

species	wavelength	transition state	refs
CO	283	$b^3\Sigma^+ \rightarrow a^3\Pi_r$ (0,0)	109
CO_2^+	289	$B^3\Sigma^+u2\Sigma^+ \rightarrow X^2\Pi_g$	110,111
CO	297	$b^3\Sigma^+ \rightarrow a^3\Pi_r$ (0,1)	110
CO_2^+	353.2	$A^2\Pi \rightarrow X^2\Pi$	112
CH	431	$A^2\Delta \rightarrow X^2\Pi$	113
CO	451	$B^1\Sigma \rightarrow a^1\Pi$ (0,0)	114
CO	484	$B^1\Sigma \rightarrow a^1\Pi$ (0,1)	115
CO	519	$B^1\Sigma \rightarrow a^1\Pi$ (0,2)	115
CO_2	559	$B^1\Sigma \rightarrow a^1\Pi$ (0,3)	115
H_α	656.3	Balmer series $3d^2D \rightarrow 2p^2P^0$	116−119
O	777.5	$3s^5S^0 \rightarrow 3p^5P$	116,117
	844.7	$3s^3S^0 \rightarrow 3p^3P$	116,117

reorganizational "shifts" within the molecule. Once rearranged, the resultant carbocation will react further to form a final product that has a different alkyl skeleton than the starting material. Our starting hypothesis is that the plasma-generated radicals (CO and O) observed in the OES analysis will initiate the HDPE attack, and the chain rupture will lead to carbocation rearrangements within the newly created sections of the polymer and result in medium-size hydrocarbon chains (shorter than the mother HDPE chain). Moreover, the employed materials are considered paraelectric perovskites.[120,121] A paraelectric material becomes polarized under an applied electric field, and it loses the polarization when the electric field is removed. In this case, such polarization can help enhance the interaction of the perovskite surface with the polar CO_2. Moreover, looking at the chemical nature of the perovskite employed, i.e., $CaTiO_3$, Ca shows the highest CO_2 adsorption of the alkaline earth metals.[122]

Hence, the enhanced activated species we observed can be formed by the dissociation reaction of the CO_2 adsorbed species[123−126] on the perovskite surface (CO_2 (ads) → CO* + O*). The improved interaction of the plasma-formed active species with the perovskite polarized surface is evident from the higher production of the main compounds in the condensate with the tailored $CaTiO_3$ that offers a higher surface area. Furthermore, recently, density functional theory (DFT) modeling has shown that accumulated surface charge on different surfaces increases the CO_2 adsorption strength and decreases the CO_2 dissociation barrier.[127]

To observe experimentally the benefit of the perovskite, we calculated the contribution of the perovskite by subtracting the intensity of some selected species in the perovskite-plasma system from the intensity of the plasma-only system (see Figure 7). Interestingly, for the same catalyst and different stage setup, the intensity of plasma species was slightly lower in the gas phase for a boat setup compared to the capillary setup, which correlates directly with the experimental observations, suggesting the involvement of these important plasma species on the surface of perovskites, leading to better performance (see Figure 7b). It is evident that the tailored $CaTiO_3$ perovskite, with a higher surface area, improves the intensity of the activated species (both CO and O), which we propose as initiators of polymer decomposition by random scission that led to linear hydrocarbons and aromatics. These are most probably formed by secondary reactions such as hydrogen and carbon transfer within intermediate alkenes, resulting in rearranged hydrocarbon chains that can be used as platforms/specialty chemicals or fuel. While much work still needs to be done, this preliminary understanding can help set up the basis for future studies using plasma-responsive materials such as perovskites.

3.6. Effect of Stage Setup. Based on the best performance, commercial and tailored $CaTiO_3$ were employed for studying the effect of stage setup on HDPE decomposition, previously presented in Figure 2(b,c), at two different flow rates of 10 and 50 sccm. The boat setup exhibited a higher amount of condensates compared to the capillary setup for both commercial and tailored $CaTiO_3$ (see Figure 8(a,b)). The comparative analysis was also investigated on the gas phase using optical emission spectroscopy. Interestingly, the gas phase showed a lower intensity (au) for important plasma species such as the CH band, H_α band, and O band for the boat setup compared to the capillary setup, suggesting increased activity on the perovskite surface, enhancing the condensate yield (see Figures 7(b) and S6). When compared to tailored vs commercial $CaTiO_3$, it can be seen that the tailored perovskite enhanced the yield for C13 and a lower carbon number, and the higher catalytic performance for tailored $CaTiO_3$ can be observed due to the higher surface area (m^2/g). The higher catalytic performance of the tailored

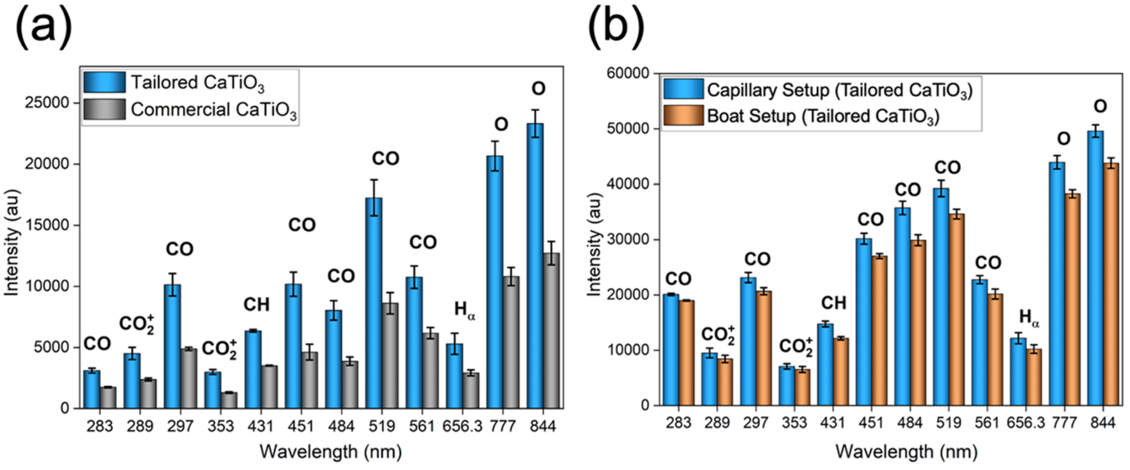

Figure 7. Comparison of the intensity of selected plasma-generated species when employing (a) conducted for a capillary stage setup with commercial vs tailored $CaTiO_3$, (b) for capillary vs boat stage setup with tailored $CaTiO_3$.

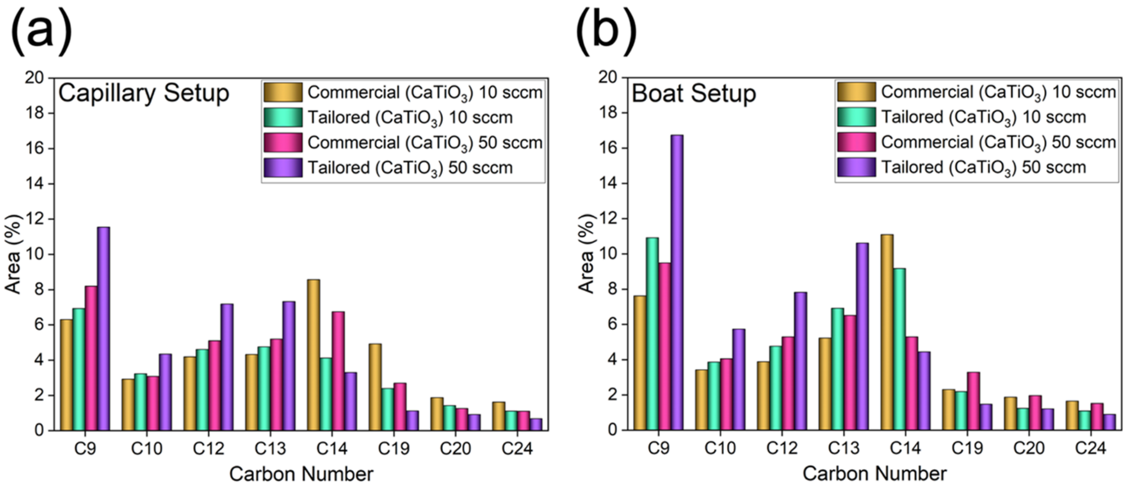

Figure 8. Effect of stage configuration on product distribution for HDPE decomposition: (a) capillary setup and (b) boat setup ($CaTiO_3$) at various flow rates for 60 min of reaction time.

material can be further supported by the XRD analysis, which shows that the tailored $CaTiO_3$ has a lower crystallinity leading to plane defects on the perovskite structure that offer more active sites for reactions to occur (see Figure S3(b)). These textural properties directly correlate with the effect of residence time, as the different stage setup offers enhancement toward selective products, such as a lower residence time leading to a high fraction of shorter chain carbon (C9−C13 products) and a higher residence time leading to more long-chain carbon (C14+ products).

3.7. Technology Maturity. To the best of our knowledge, in comparison to conventional thermal pyrolysis, which occurs at high temperatures (500−800 °C),[91] the main advantage of the presented work is the possible decomposition of HDPE at a lower temperature (250 °C) compared to the thermal route. (1) This, based on the literature, is generally favorable for decomposing toxic gases from mixed plastic waste;[128] and (2) this mild energy process can limit the production of free chlorine from HCl.[128] An added advantage also is the use of a material that can respond to an electric field, in this case, a perovskite. A possible main disadvantage is the high electricity requirement being RF plasma.[128] However, it is important to note that electron-mediated technologies (such as plasma) can be turned on/off instantly and are compatible with renewable power sources, such as solar or wind, making this process sustainable and economical when pairing with renewables for carbon restoration.[2] A particular advantage of the conversion process developed in this research is the direct production of molecules that possess favorable fuel properties. A common drawback in biofuel production, whether using chemical or biological approaches, is the need to conduct additional steps (such as hydrogenation) to convert the molecules into more suitable candidates. Herein, we presented a one-pot, low-temperature, and fast process to upcycle HDPE. The presented process can help set up the basis for future optimization for scale-up and deployment when using novel materials responsive to electric field disturbances. Currently, there is a demand for technology maturity in association with plasma decomposition; however, we are still in the very early stages. Nevertheless, the capability of plasma is well-acknowledged by the industry and scientific community.[129]

4. CONCLUSIONS

Herein, we present the possibility of taking advantage of CO_2 plasma-generated species when perovskites are used, a material responsive to electrical inducement. We demonstrated that CO_2 plasma degradation of HDPE leads to high CO_2 conversions and is enhanced by the presence of perovskites, which greatly affect the product distribution. We observed an increase in the presence of plasma-activated species when the perovskite is in the reaction chamber. The effect of the perovskite led to an improved intensity of the species prone to initiating the HDPE decomposition such as O atoms and CO. These CO2 plasma-generated initiators direct random scissions, resulting in condensates with potential use as synthetic fuel since the product stream comprises C_5−C_{11} naphtha, which can be blended into gasoline; C_9−C_{20} diesel, which has a high cetane number; and C_{20+} waxes, which can also be converted into diesel through hydrocracking. We expect this work to enable the development of tailored materials that are responsive to electric fields.

■ ASSOCIATED CONTENT

Supporting Information

The Supporting Information is available free of charge at https://pubs.acs.org/doi/10.1021/acs.iecr.3c02403.

BET surface area details for commercial and tailored perovskites; X-ray diffraction pattern for employed perovskites; SEM images for perovskites after plasma exposure; product distribution (carbon number) for plasma only; commercial and tailored $CaTiO_3$; state-of-the-art table for HDPE thermal and plasma catalysis; and predicted blend properties for employed catalysts (PDF)

■ AUTHOR INFORMATION

Corresponding Author

Maria L. Carreon − *Department of Mechanical & Industrial Engineering, University of Massachusetts Lowell, Lowell, Massachusetts 01854, United States;* orcid.org/0000-0002-2717-1577; Email: maria_carreon@uml.edu

Authors

Fnu Gorky − *Department of Mechanical & Industrial Engineering, University of Massachusetts Lowell, Lowell, Massachusetts 01854, United States*

Apolo Nambo − *Bert Thin Films, LLC, Louisville, Kentucky 40208, United States*

Travis J. Kessler − *Department of Electrical & Computer Engineering, University of Massachusetts Lowell, Lowell, Massachusetts 01854, United States*

J. Hunter Mack − *Department of Mechanical & Industrial Engineering, University of Massachusetts Lowell, Lowell, Massachusetts 01854, United States*

Complete contact information is available at:
https://pubs.acs.org/10.1021/acs.iecr.3c02403

Notes

The authors declare no competing financial interest.

■ ACKNOWLEDGMENTS

M.L.C. acknowledges NSF-CBET award No.1947303, NSF-CAREER award No. 2235247, and Department of Energy Office of Science DE-SC0023261.

■ REFERENCES

(1) Kleij, A. W.; North, M.; Urakawa, A. CO2 Catalysis. *ChemSusChem* **2017**, *10* (6), 1036−1038.

(2) Bogaerts, A.; Tu, X.; Whitehead, J. C.; Centi, G.; Lefferts, L.; Guaitella, O.; Azzolina-Jury, F.; Kim, H.-H.; Murphy, A. B.; Schneider, W. F.; et al. The 2020 plasma catalysis roadmap. *J. Phys. D: Appl. Phys.* **2020**, *53* (44), No. 443001.

(3) Hall-Spencer, J. M.; Harvey, B. P. Ocean acidification impacts on coastal ecosystem services due to habitat degradation. *Emerging Top. Life Sci.* **2019**, *3* (2), 197−206.

(4) Duyar, M. S.; Treviño, M. A. A.; Farrauto, R. J. Dual function materials for CO2 capture and conversion using renewable H2. *Appl. Catal., B* **2015**, *168*−*169*, 370−376.

(5) Aresta, M.; Dibenedetto, A. Utilisation of CO2 as a chemical feedstock: opportunities and challenges. *Dalton Trans.* **2007**, No. 28, 2975−2992.

(6) Andrady, A. L.; Neal, M. A. Applications and societal benefits of plastics. *Philos. Trans. R. Soc., B* **2009**, *364* (1526), 1977−1984.

(7) Geyer, R.; Jambeck, J. R.; Law, K. L. Production, use, and fate of all plastics ever made. *Sci. Adv.* **2017**, *3* (7), No. e1700782.

(8) Andrady, A. L. *Plastics and the Environment*; John Wiley & Sons: NJ, 2003; Vol. *1*, p 674.

(9) Law, K. L. Plastics in the marine environment. *Ann. Rev. Mar. Sci.* **2017**, *9*, 205−229.

(10) Silvarrey, L. D.; Phan, A. N. Kinetic study of municipal plastic waste. *Int. J. Hydrogen Energy* **2016**, *41* (37), 16352−16364.

(11) U.S. Environmental Protection Agency (EPA). *Energy and the Environment* 2016.

(12) Schyns, Z. O. G.; Shaver, M. P. Mechanical recycling of packaging plastics: A review. *Macromol. Rapid Commun.* **2021**, *42* (3), No. 2000415.

(13) Costa, C. S.; Muñoz, M.; Ribeiro, M. R.; Silva, J. M. H-USY and H-ZSM-5 zeolites as catalysts for HDPE conversion under a hydrogen reductive atmosphere. *Sustainable Energy Fuels* **2021**, *5* (4), 1134−1147.

(14) Di, J.; Reck, B. K.; Miatto, A.; Graedel, T. E. United States plastics: Large flows, short lifetimes, and negligible recycling. *Resour., Conserv. Recycl.* **2021**, *167*, No. 105440.

(15) Al-Salem, S. M.; Lettieri, P.; Baeyens, J. Recycling and recovery routes of plastic solid waste (PSW): A review. *Waste Manage.* **2009**, *29* (10), 2625−2643.

(16) Lamar, Y. R.; Noboa, J.; Miranda, A. S. T.; Streitwieser, D. A. Conversion of PP, HDPE and LDPE plastics into liquid fuels and chemical precursors by thermal cracking. *J. Polym. Environ.* **2021**, *29* (12), 3842−3853.

(17) Vogt, B. D.; Stokes, K. K.; Kumar, S. K. Why is recycling of postconsumer plastics so challenging? *ACS Appl. Polym. Mater.* **2021**, *3* (9), 4325−4346.

(18) Huang, J.; Zhang, Q.; Zhao, M.; Wei, F. A review of the large-scale production of carbon nanotubes: The practice of nanoscale process engineering. *Chin. Sci. Bull.* **2012**, *57* (2), 157−166.

(19) Dogu, O.; Pelucchi, M.; Van de Vijver, R.; Van Steenberge, P. H. M.; D'Hooge, D. R.; Cuoci, A.; Mehl, M.; Frassoldati, A.; Faravelli, T.; Van Geem, K. M. The chemistry of chemical recycling of solid plastic waste via pyrolysis and gasification: State-of-the-art, challenges, and future directions. *Prog. Energy Combust. Sci.* **2021**, *84*, No. 100901.

(20) Tennakoon, A.; Wu, X.; Paterson, A. L.; Patnaik, S.; Pei, Y.; LaPointe, A. M.; Ammal, S. C.; Hackler, R. A.; Heyden, A.; Slowing, I. I.; et al. Catalytic upcycling of high-density polyethylene via a processive mechanism. *Nat. Catal.* **2020**, *3* (11), 893−901.

(21) Korley, L. T. J.; Epps, T. H., Iii; Helms, B. A.; Ryan, A. J. Toward polymer upcycling—adding value and tackling circularity. *Science* **2021**, *373* (6550), 66−69.

(22) Chen, X.; Wang, Y.; Zhang, L. Recent progress in the chemical upcycling of plastic wastes. *ChemSusChem* **2021**, *14* (19), 4137−4151.

(23) Chen, H.; Wan, K.; Zhang, Y.; Wang, Y. Waste to wealth: chemical recycling and chemical upcycling of waste plastics for a great future. *ChemSusChem* **2021**, *14* (19), 4123−4136.

(24) Yao, L.; King, J.; Wu, D.; Chuang, S. S. C.; Peng, Z. Non-thermal plasma-assisted hydrogenolysis of polyethylene to light hydrocarbons. *Catal. Commun.* **2021**, *150*, No. 106274.

(25) Yao, L.; King, J.; Wu, D.; Ma, J.; Li, J.; Xie, R.; Chuang, S. S. C.; Miyoshi, T.; Peng, Z. Non-thermal plasma-assisted rapid hydrogenolysis of polystyrene to high yield ethylene. *Nat. Commun.* **2022**, *13* (1), No. 885.

(26) Al-Salem, S. M. Thermal pyrolysis of high density polyethylene (HDPE) in a novel fixed bed reactor system for the production of high value gasoline range hydrocarbons (HC). *Process Saf. Environ. Prot.* **2019**, *127*, 171−179.

(27) Mastral, F.; Esperanza, E.; Garcıa, P.; Juste, M. Pyrolysis of high-density polyethylene in a fluidised bed reactor. Influence of the temperature and residence time. *J. Anal. Appl. Pyrolysis* **2002**, *63* (1), 1−15.

(28) Martínez, L.; Aguado, A.; Moral, A.; Irusta, R. Fluidized bed pyrolysis of HDPE: A study of the influence of operating variables and the main fluidynamic parameters on the composition and production of gases. *Fuel Process. Technol.* **2011**, *92* (2), 221−228.

(29) Kumar, S.; Singh, R. Optimization of process parameters by response surface methodology (RSM) for catalytic pyrolysis of waste high-density polyethylene to liquid fuel. *J. Environ. Chem. Eng.* **2014**, *2* (1), 115−122.

(30) Mastral, F.; Esperanza, E.; Berrueco, C.; Juste, M.; Ceamanos, J. Fluidized bed thermal degradation products of HDPE in an inert atmosphere and in air−nitrogen mixtures. *J. Anal. Appl. Pyrolysis* **2003**, *70* (1), 1−17.

(31) Al-Salem, S. M.; Lettieri, P. Kinetic study of high density polyethylene (HDPE) pyrolysis. *Chem. Eng. Res. Des.* **2010**, *88* (12), 1599−1606.

(32) Gascoin, N.; Navarro-Rodriguez, A.; Gillard, P.; Mangeot, A. Kinetic modelling of high density polyethylene pyrolysis: Part 1. Comparison of existing models. *Polym. Degrad. Stab.* **2012**, *97* (8), 1466−1474.

(33) Liu, X.; Li, X.; Liu, J.; Wang, Z.; Kong, B.; Gong, X.; Yang, X.; Lin, W.; Guo, L. Study of high density polyethylene (HDPE) pyrolysis with reactive molecular dynamics. *Polym. Degrad. Stab.* **2014**, *104*, 62−70.

(34) Kayacan, I.; Doğan, Ö. Pyrolysis of low and high density polyethylene. Part I: non-isothermal pyrolysis kinetics. *Energy Sources, Part A* **2008**, *30* (5), 385−391.

(35) Li, H.; Mašek, O.; Harper, A.; Ocone, R. Kinetic study of pyrolysis of high-density polyethylene (HDPE) waste at different bed

thickness in a fixed bed reactor. *Can. J. Chem. Eng.* **2021**, *99* (8), 1733−1744.

(36) Cheng, L.; Gu, J.; Wang, Y.; Zhang, J.; Yuan, H.; Chen, Y. Polyethylene high-pressure pyrolysis: Better product distribution and process mechanism analysis. *Chem. Eng. J.* **2020**, *385*, No. 123866.

(37) Pichler, C. M.; Bhattacharjee, S.; Rahaman, M.; Uekert, T.; Reisner, E. Conversion of polyethylene waste into gaseous hydrocarbons via integrated tandem chemical−photo/electrocatalytic processes. *ACS Catal.* **2021**, *11* (15), 9159−9167.

(38) Li, C.; Zhang, C.; Gholizadeh, M.; Hu, X. Different reaction behaviours of light or heavy density polyethylene during the pyrolysis with biochar as the catalyst. *J. Hazard. Mater.* **2020**, *399*, No. 123075.

(39) Jaafar, Y.; Abdelouahed, L.; El Hage, R.; El Samrani, A.; Taouk, B. Pyrolysis of common plastics and their mixtures to produce valuable petroleum-like products. *Polym. Degrad. Stab.* **2022**, *195*, No. 109770.

(40) Diaz-Silvarrey, L. S.; Zhang, K.; Phan, A. N. Monomer recovery through advanced pyrolysis of waste high density polyethylene (HDPE). *Green Chem.* **2018**, *20* (8), 1813−1823.

(41) Saleem, F.; Harris, J.; Zhang, K.; Harvey, A. Non-thermal plasma as a promising route for the removal of tar from the product gas of biomass gasification−a critical review. *Chem. Eng. J.* **2020**, *382*, No. 122761.

(42) Kwon, S.; Im, S.-k. Feasibility of non-thermal plasma gasification for a waste-to-energy power plant. *Energy Convers. Manage.* **2022**, *251*, No. 114978.

(43) Nitsche, T.; Unger, C.; Weidner, E. Plasma catalytical reactors for atmospheric gas conversions. *Chem. Ing. Tech.* **2018**, *90* (10), 1453−1464.

(44) Xu, S.; Chansai, S.; Stere, C.; Inceesungvorn, B.; Goguet, A.; Wangkawong, K.; Taylor, S. F. R.; Al-Janabi, N.; Hardacre, C.; Martin, P. A.; Fan, X. Sustaining metal−organic frameworks for water−gas shift catalysis by non-thermal plasma. *Nat. Catal.* **2019**, *2* (2), 142−148.

(45) Gorky, F.; Lucero, J. M.; Crawford, J. M.; Blake, B.; Carreon, M. A.; Carreon, M. L. Plasma-Induced Catalytic Conversion of Nitrogen and Hydrogen to Ammonia over Zeolitic Imidazolate Frameworks ZIF-8 and ZIF-67. *ACS Appl. Mater. Interfaces* **2021**, *13* (18), 21338−21348.

(46) Ceamanos, J.; Mastral, J.; Millera, A.; Aldea, M. Kinetics of pyrolysis of high density polyethylene. Comparison of isothermal and dynamic experiments. *J. Anal. Appl. Pyrolysis* **2002**, *65* (2), 93−110.

(47) Sobeih, K. L.; Baron, M.; Gonzalez-Rodriguez, J. Recent trends and developments in pyrolysis−gas chromatography. *J. Chromatogr. A* **2008**, *1186* (1−2), 51−66.

(48) Weitkamp, J.; Puppe, L. *Catalysis and Zeolites: Fundamentals and Applications*; Springer Science & Business Media: Verlag Berlin Heidelberg, 1999; Vol. *1*, p 453.

(49) Vogt, E. T. C.; Weckhuysen, B. M. Fluid catalytic cracking: recent developments on the grand old lady of zeolite catalysis. *Chem. Soc. Rev.* **2015**, *44* (20), 7342−7370.

(50) Biswas, A. N.; Winter, L. R.; Loenders, Br.; Xie, Z.; Bogaerts, A.; Chen, J. G. Oxygenate Production from Plasma-Activated Reaction of CO2 and Ethane. *ACS Energy Lett.* **2022**, *7*, 236−241.

(51) Nguyen, H. M.; Carreon, M. L. Non-thermal Plasma-Assisted Deconstruction of High-Density Polyethylene to Hydrogen and Light Hydrocarbons over Hollow ZSM-5 Microspheres. *ACS Sustainable Chem. Eng.* **2022**, *10* (29), 9480−9491.

(52) Sakata, Y.; Uddin, M. A.; Muto, A.; Kanada, Y.; Koizumi, K.; Murata, K. Catalytic degradation of polyethylene into fuel oil over mesoporous silica (KFS-16) catalyst. *J. Anal. Appl. Pyrolysis* **1997**, *43* (1), 15−25.

(53) Kao, K. C. *Dielectric Phenomena in Solids*; Elsevier, 2004.

(54) Yi, H. T.; Choi, T.; Choi, S. G.; Oh, Y. S.; Cheong, S. W. Mechanism of the switchable photovoltaic effect in ferroelectric BiFeO3. *Adv. Mater.* **2011**, *23* (30), 3403−3407.

(55) Ahn, C. H.; Rabe, K.; Triscone, J.-M. Ferroelectricity at the nanoscale: local polarization in oxide thin films and heterostructures. *Science* **2004**, *303* (5657), 488−491.

(56) Khan, M.; Bhansali, U. S.; Alshareef, H. N. Fabrication and characterization of all-polymer, transparent ferroelectric capacitors on flexible substrates. *Org. Electron.* **2011**, *12* (12), 2225−2229.

(57) Mehta, P.; Barboun, P.; Go, D. B.; Hicks, J. C.; Schneider, W. F. Catalysis enabled by plasma activation of strong chemical bonds: a review. *ACS Energy Lett.* **2019**, *4* (5), 1115−1133.

(58) Neyts, E. C. Plasma-surface interactions in plasma catalysis. *Plasma Chem. Plasma Process.* **2016**, *36*, 185−212.

(59) Bhattar, S.; Abedin, M. A.; Kanitkar, S.; Spivey, J. J. A review on dry reforming of methane over perovskite derived catalysts. *Catal. Today* **2021**, *365*, 2−23.

(60) de Caprariis, B.; de Filippis, P.; Palma, V.; Petrullo, A.; Ricca, A.; Ruocco, C.; Scarsella, M. Rh, Ru and Pt ternary perovskites type oxides BaZr (1-x) MexO3 for methane dry reforming. *Appl. Catal., A* **2016**, *517*, 47−55.

(61) Bal, K. M.; Huygh, S.; Bogaerts, A.; Neyts, E. C. Effect of plasma-induced surface charging on catalytic processes: application to CO2 activation. *Plasma Sources Sci. Technol.* **2018**, *27* (2), No. 024001.

(62) Grote, M.; Williams, I.; Preston, J. Direct carbon dioxide emissions from civil aircraft. *Atmos. Environ.* **2014**, *95*, 214−224.

(63) Zhang, L.; Butler, T. L.; Yang, B. Recent trends, opportunities and challenges of sustainable aviation fuel. *Green Energy Sustainability* **2020**, 85−110.

(64) Zheng, L.; Singh, P.; Cronly, J.; Ubogu, E. A.; Ahmed, I.; Ling, C.; Zhang, Y.; Khandelwal, B. Impact of aromatic structures and content in formulated fuel for jet engine applications on particulate matter emissions. *J. Energy Resour. Technol.* **2021**, *143* (12), No. 122301.

(65) Hou, Q.; Zhen, M.; Qian, H.; Nie, Y.; Bai, X.; Xia, T.; Rehman, M. L. U.; Li, Q.; Ju, M. Upcycling and catalytic degradation of plastic wastes. *Cell Rep. Phys. Sci.* **2021**, 2 (8), No. 100514, DOI: 10.1016/j.xcrp.2021.100514.

(66) Jehanno, C.; Alty, J. W.; Roosen, M.; De Meester, S.; Dove, A. P.; Chen, E. Y. X.; Leibfarth, F. A.; Sardon, H. Critical advances and future opportunities in upcycling commodity polymers. *Nature* **2022**, *603* (7903), 803−814.

(67) Han, C.; Liu, J.; Yang, W.; Wu, Q.; Yang, H.; Xue, X. Photocatalytic activity of CaTiO 3 synthesized by solid state, sol−gel and hydrothermal methods. *J. Sol−Gel Sci. Technol.* **2017**, *81*, 806−813.

(68) Zhao, H.; Duan, Y.; Sun, X. Synthesis and characterization of CaTiO 3 particles with controlled shape and size. *New J. Chem.* **2013**, *37* (4), 986−991.

(69) Shah, J. R.; Gorky, F.; Lucero, J.; Carreon, M. A.; Carreon, M. L. Ammonia synthesis via atmospheric plasma catalysis: zeolite 5A, a case of study. *Ind. Eng. Chem. Res.* **2020**, *59* (11), 5167−5176.

(70) Saldana, D. A.; Starck, L.; Mougin, P.; Rousseau, B.; Pidol, L.; Jeuland, N.; Creton, B. Flash point and cetane number predictions for fuel compounds using quantitative structure property relationship (QSPR) methods. *Energy Fuels* **2011**, *25* (9), 3900−3908.

(71) Piloto-Rodríguez, R.; Sánchez-Borroto, Y.; Lapuerta, M.; Goyos-Pérez, L.; Verhelst, S. Prediction of the cetane number of biodiesel using artificial neural networks and multiple linear regression. *Energy Convers. Manage.* **2013**, *65*, 255−261.

(72) Freedman, B.; Bagby, M. O. Predicting cetane numbers of n-alcohols and methyl esters from their physical properties. *J. Am. Oil Chem. Soc.* **1990**, *67* (9), 565−571.

(73) Barra, I.; Kharbach, M.; Qannari, E. M.; Hanafi, M.; Cherrah, Y.; Bouklouze, A. Predicting cetane number in diesel fuels using FTIR spectroscopy and PLS regression. *Vib. Spectrosc.* **2020**, *111*, No. 103157.

(74) Whitmore, L. S.; Davis, R. W.; McCormick, R. L.; Gladden, J. M.; Simmons, B. A.; George, A.; Hudson, C. M. BioCompoundML: a general biofuel property screening tool for biological molecules using Random Forest Classifiers. *Energy Fuels* **2016**, *30* (10), 8410−8418.

(75) Smolenskii, E. A.; Bavykin, V. M.; Ryzhov, A. N.; Slovokhotova, O. L.; Chuvaeva, I. V.; Lapidus, A. L. Cetane numbers of

hydrocarbons: calculations using optimal topological indices. *Russ. Chem. Bull.* **2008**, *57*, 461−467.

(76) John, P. C. S.; Kairys, P.; Das, D. D.; McEnally, C. S.; Pfefferle, L. D.; Robichaud, D. J.; Nimlos, M. R.; Zigler, B. T.; McCormick, R. L.; Foust, T. D.; et al. A quantitative model for the prediction of sooting tendency from molecular structure. *Energy Fuels* **2017**, *31* (9), 9983−9990, DOI: 10.1021/acs.energyfuels.7b00616.

(77) Meng, X.; Jia, M.; Wang, T. Neural network prediction of biodiesel kinematic viscosity at 313 K. *Fuel* **2014**, *121*, 133−140.

(78) Ren, Y.; Liu, H.; Yao, X.; Liu, M.; Hu, Z.; Fan, B. The accurate QSPR models for the prediction of nonionic surfactant cloud point. *J. Colloid Interface Sci.* **2006**, *302* (2), 669−672.

(79) Schweidtmann, A. M.; Rittig, J. G.; König, A.; Grohe, M.; Mitsos, A.; Dahmen, M. Graph neural networks for prediction of fuel ignition quality. *Energy Fuels* **2020**, *34* (9), 11395−11407.

(80) Kessler, T.; John, P. C. S.; Zhu, J.; McEnally, C. S.; Pfefferle, L. D.; Mack, J. H. A comparison of computational models for predicting yield sooting index. *Proc. Combust. Inst.* **2021**, *38* (1), 1385−1393.

(81) Wang, Y.; Dong, W.; Liang, W.; Yang, B.; Law, C. K. Predicting octane number from species profiles: A deep learning model. *Proc. Combust. Inst.* **2023**, *39* (4), 5269−5277.

(82) Kessler, T.; Sacia, E. R.; Bell, A. T.; Mack, J. H. Artificial neural network based predictions of cetane number for furanic biofuel additives. *Fuel* **2017**, *206*, 171−179.

(83) SubLaban, A.; Kessler, T. J.; Van Dam, N.; Mack, J. H. Artificial Neural Network Models for Octane Number and Octane Sensitivity: A Quantitative Structure Property Relationship Approach to Fuel Design. *J. Energy Resour. Technol.* **2023**, *145* (10), No. 102302.

(84) Kessler, T.; Schwartz, T.; Wong, H.-W.; Mack, J. H. In *Evaluating Diesel/Biofuel Blends Using Artificial Neural Networks and Linear/Nonlinear Equations*, ASME 2021 Internal Combustion Engine Division Fall Technical Conference; American Society of Mechanical Engineers, 2021; V001T004A009.

(85) Cabanes, A.; Valdés, F. J.; Fullana, A. A review on VOCs from recycled plastics. *Sustainable Mater. Technol.* **2020**, *25*, No. e00179.

(86) Briker, Y.; Ring, Z.; Iacchelli, A.; McLean, N.; Rahimi, P. M.; Fairbridge, C.; Malhotra, R.; Coggiola, M. A.; Young, S. E. Diesel fuel analysis by GC− FIMS: Aromatics, n-paraffins, and isoparaffins. *Energy Fuels* **2001**, *15* (1), 23−37.

(87) Prak, D. J. L.; Cowart, J. S.; Hamilton, L. J.; Hoang, D. T.; Brown, E. K.; Trulove, P. C. Development of a surrogate mixture for algal-based hydrotreated renewable diesel. *Energy Fuels* **2013**, *27* (2), 954−961.

(88) Bhoi, P. R.; Rahman, M. H. Hydrocarbons recovery through catalytic pyrolysis of compostable and recyclable waste plastics using a novel desk-top staged reactor. *Environ. Technol. Innovation* **2022**, *27*, No. 102453.

(89) Blakey, S.; Rye, L.; Wilson, C. W. Aviation gas turbine alternative fuels: A review. *Proc. Combust. Inst.* **2011**, *33* (2), 2863−2885.

(90) Gardler, T. F. Chemical Characterization of Aviation Fuels by Gas Chromatography-Mass Spectrometry. Ph.D. Thesis. North Carolina Agricultural and Technical State University, 2014.

(91) Olazar, M.; Lopez, G.; Amutio, M.; Elordi, G.; Aguado, R.; Bilbao, J. Influence of FCC catalyst steaming on HDPE pyrolysis product distribution. *J. Anal. Appl. Pyrolysis* **2009**, *85* (1−2), 359−365.

(92) Preuss, R.; Angerer, J.; Drexler, H. Naphthalene—an environmental and occupational toxicant. *Int. Arch. Occup. Environ. Health* **2003**, *76*, 556−576.

(93) Kumar, S.; Singh, R. K. Thermolysis of high-density polyethylene to petroleum products. *J. Pet. Eng.* **2013**, *2013*, No. 987568, DOI: 10.1155/2013/987568.

(94) Bhownath, R. The Use of n-Dodecane as a Solvent in the Extraction of Light Alcohols from Water. Ph.D. Thesis. University of Kwa-Zulu Natal, 2008.

(95) Ma, Y.; Harding, J. D.; Tu, X. Catalyst-free low temperature conversion of n-dodecane for co-generation of COx-free hydrogen and C2 hydrocarbons using a gliding arc plasma. *Int. J. Hydrogen Energy* **2019**, *44* (48), 26158−26168.

(96) Ahmad, I.; Khan, M. I.; Khan, H.; Ishaq, M.; Tariq, R.; Gul, K.; Ahmad, W. Influence of metal-oxide-supported bentonites on the pyrolysis behavior of polypropylene and high-density polyethylene *J. Appl. Polym. Sci.* 2015, *1321* DOI: 10.1002/app.41221.

(97) Gunasekara, S. N.; Kumova, S.; Chiu, J. N.; Martin, V. Experimental phase diagram of the dodecane−tridecane system as phase change material in cold storage. *Int. J. Refrig.* **2017**, *82*, 130−140.

(98) Bo, H.; Gustafsson, E. M.; Setterwall, F. Tetradecane and hexadecane binary mixtures as phase change materials (PCMs) for cool storage in district cooling systems. *Energy* **1999**, *24* (12), 1015−1028.

(99) Commission Implementing Regulation (EU) No 872/2012 of 1 October 2012 adopting the list of flavouring substances provided for by Regulation (EC) No 2232/96 of the European Parliament and of the Council, introducing it in Annex I to Regulation (EC) No 1334/2008 of the European Parliament and of the Council and repealing Commission Regulation (EC) No 1565/2000 and Commission Decision 1999/217/EC Text with EEA relevance. In L267.

(100) Dutra, C.; Pezo, D.; de Alvarenga Freire, M. T.; Nerín, C.; Reyes, F. G. R. Determination of volatile organic compounds in recycled polyethylene terephthalate and high-density polyethylene by headspace solid phase microextraction gas chromatography mass spectrometry to evaluate the efficiency of recycling processes. *J. Chromatogr. A* **2011**, *1218* (10), 1319−1330.

(101) Jan, M. R.; Shah, J.; Gulab, H. Catalytic degradation of waste high-density polyethylene into fuel products using BaCO3 as a catalyst. *Fuel Process. Technol.* **2010**, *91* (11), 1428−1437.

(102) Madruga, S.; Haruki, N.; Horibe, A. Experimental and numerical study of melting of the phase change material tetracosane. *Int. Commun. Heat Mass Transfer* **2018**, *98*, 163−170.

(103) Jamalzade, E.; Kashkooli, K.; Griffin, L.; van Walsum, G. P.; Schwartz, T. J. Production of jet-fuel-range molecules from biomass-derived mixed acids. *React. Chem. Eng.* **2021**, *6* (5), 845−857.

(104) Haze, S.; Sakai, K.; Gozu, Y. Effects of fragrance inhalation on sympathetic activity in normal adults. *Jpn. J. Pharmacol.* **2002**, *90* (3), 247−253.

(105) Li, H.; Liu, X.; Fang, G. Preparation and characteristics of n-nonadecane/cement composites as thermal energy storage materials in buildings. *Energy Build.* **2010**, *42* (10), 1661−1665.

(106) Ng, D. K. S.; Ng, K. S.; Ng, R. T. L. Integrated Biorefineries. In *Encyclopedia of Sustainable Technologies*; Elsevier, 2017; pp 299−314.

(107) Singh, H.; Blennow, A.; Gupta, A. D.; Kaur, P.; Dhillon, B.; Sodhi, N. S.; Dubey, P. K. Pulsed light, pulsed electric field and cold plasma modification of starches: technological advancements & effects on functional properties. *J. Food Meas. Charact.* **2022**, *16* (5), 4092−4109.

(108) Runion, H. E. Benzene in gasoline. *Am. Ind. Hyg. Assoc. J.* **1975**, *36* (5), 338−350.

(109) Zhang, D.; Huang, Q.; Devid, E. J.; Schuler, E.; Shiju, N. R.; Rothenberg, G.; van Rooij, G.; Yang, R.; Liu, K.; Kleyn, A. W. Tuning of conversion and optical emission by electron temperature in inductively coupled CO2 plasma. *J. Phys. Chem. C* **2018**, *122* (34), 19338−19347.

(110) Kraus, M.; Egli, W.; Haffner, K.; Eliasson, B.; Kogelschatz, U.; Wokaun, A. Investigation of mechanistic aspects of the catalytic CO 2 reforming of methane in a dielectric-barrier discharge using optical emission spectroscopy and kinetic modeling. *Phys. Chem. Chem. Phys.* **2002**, *4* (4), 668−675.

(111) Li, Z.; Niu, D.; Gu, H.; Wu, X.; Huang, Y.; Zhong, J.; Cui, J. Modeling the CO 2+ Ultraviolet Doublet Emission from Mars with a Multi-Instrument MAVEN Data Set. *Remote Sens.* **2022**, *14* (7), No. 1705.

(112) Reyes, P. G.; Mendez, E. F.; Osorio-Gonzalez, D.; Castillo, F.; Martínez, H. Optical emission spectroscopy of CO2 glow discharge at low pressure. *Phys. Status Solidi C* **2008**, *5* (4), 907−910.

(113) Kang, S.; Mauchauffé, R.; You, Y. S.; Moon, S. Y. Insights into the role of plasma in atmospheric pressure chemical vapor deposition of titanium dioxide thin films. *Sci. Rep.* **2018**, *8* (1), No. 16684.

(114) Bougdira, J.; Remy, M.; Alnot, P.; Bruch, C.; Kruger, J. K.; Chatei, H.; Derkaoui, J. Combined effect of nitrogen and pulsed microwave plasma on diamond growth using CH4−CO2 gas mixture. *Thin Solid Films* **1998**, *325* (1−2), 7−13.

(115) Goujon, M.; Belmonte, T.; Henrion, G. OES and FTIR diagnostics of HMDSO/O2 gas mixtures for SiOx deposition assisted by RF plasma. *Surf. Coat. Technol.* **2004**, *188-189*, 756−761.

(116) McConkey, J. W.; Malone, C. P.; Johnson, P. V.; Winstead, C.; McKoy, V.; Kanik, I. Electron impact dissociation of oxygen-containing molecules−A critical review. *Phys. Rep.* **2008**, *466* (1−3), 1−103.

(117) Wang, L.; Yi, Y.; Wu, C.; Guo, H.; Tu, X. One-step reforming of CO2 and CH4 into high-value liquid chemicals and fuels at room temperature by plasma-driven catalysis. *Angew. Chem.* **2017**, *129* (44), 13867−13871.

(118) Gorky, F.; Nambo, A.; Carreon, M. L. Cold plasma-Metal Organic Framework (MOF)-177 breathable system for atmospheric remediation. *J. CO2 Util.* **2021**, *51*, No. 101642.

(119) Kondo, M.; Fukawa, M.; Guo, L.; Matsuda, A. High rate growth of microcrystalline silicon at low temperatures. *J. Non-Cryst. Solids* **2000**, *266-269*, 84−89.

(120) Rupprecht, G.; Bell, R. O. Dielectric constant in paraelectric perovskites. *Phys. Rev.* **1964**, *135* (3A), No. A748.

(121) Lemanov, V. V.; Sotnikov, A. V.; Smirnova, E. P.; Weihnacht, M.; Kunze, R. Perovskite CaTiO3 as an incipient ferroelectric. *Solid State Commun.* **1999**, *110* (11), 611−614.

(122) Da Silva, A. L.; Wu, L.; Caliman, L. B.; Castro, R. H. R.; Navrotsky, A.; Gouvêa, D. Energetics of CO 2 and H 2 O adsorption on alkaline earth metal doped TiO 2. *Phys. Chem. Chem. Phys.* **2020**, *22* (27), 15600−15607.

(123) Hueso, J. L.; González-Elipe, A. R.; Cotrino, J.; Caballero, A. Plasma chemistry of NO in complex gas mixtures excited with a surfatron launcher. *J. Phys. Chem. A* **2005**, *109* (22), 4930−4938.

(124) Aleksandrov, N. L.; Kindysheva, S. V.; Kirpichnikov, A. A.; Kosarev, I. N.; Starikovskaia, S. M.; Starikovskii, A. Y. Plasma decay in N2, CO2 and H2O excited by high-voltage nanosecond discharge. *J. Phys. D: Appl. Phys.* **2007**, *40* (15), No. 4493.

(125) Dobrea, S.; Mihaila, I.; Tiron, V.; Popa, G. Optical and mass spectrometry diagnosis of a CO2 microwave plasma discharge. *Rom. Rep. Phys.* **2014**, *66* (4), 1147−1154.

(126) Zhang, J.; Sun, J.; Gong, Y.; Wang, D.; Ma, T.; Liu, Y. A scheme for solving strongly coupled chemical reaction equations appearing in the removal of SO2 and NOx from flue gases. *Vacuum* **2008**, *83* (1), 133−137.

(127) Doherty, F.; Goldsmith, B. R. Modeling plasma-induced surface charge effects on CO2 activation by single atom catalysts supported on reducible and irreducible metal oxides. *Plasma Sources Sci. Technol.* **2023**, *32* (3), No. 034004.

(128) Solis, M.; Silveira, S. Technologies for chemical recycling of household plastics−A technical review and TRL assessment. *Waste Manage.* **2020**, *105*, 128−138.

(129) Li, S.; Liu, C.; Bogaerts, A.; Gallucci, F. special issue on CO_2 utilization with plasma technology. *J. CO2 Util.* **2022**, *61*, No. 102017.